CdS Nanoclusters: Synthesis, Characterization, Size Dependent Oscillator Strength, Temperature Shift of the Excitonic Transition Energy, and Reversible Absorbance Shift

T. Vossmeyer, L. Katsikas,† M. Giersig, I. G. Popovic,† K. Diesner,‡ A. Chemseddine, A. Eychmüller, and H. Weller*

Hahn-Meitner-Institut, Abteilung Kleinteilchenforschung Glienicker Strasse 100, 14109 Berlin, Germany

Received: April 5, 1994; In Final Form: May 6, 1994®

Improved synthetic routes and size-selective precipitation have enabled the preparation of almost monodisperse CdS clusters. Six samples of 1-thioglycerol stabilized clusters with diameters of approximately 13, 14, 16, 19, 23, and 39 Å have been prepared as fully redispersible powders and were characterized by elemental analysis, powder X-ray diffraction, electron microscopy, thermogravimetric analysis, and UV–vis spectroscopy. Small-angle X-ray scattering was used to determine the mean cluster size. The well-structured UV–vis spectra reveal that the size-dependent shift of the 1s–1s excitonic transition is in agreement with the tight-binding theory and the pseudopotential theory. Moreover, as expected by quantum mechanical calculations the oscillator strength of the transition increases proportional to $1/r^3$. UV–vis spectra taken at various temperatures between 4 and 295 K have shown that the temperature shift of the excitonic transition energy becomes stronger with decreasing particle size. Strong, reversible absorbance shifts were observed, upon transferring the clusters from their solutions onto quartz plates and vice versa.

Introduction

Nanometer-sized semiconductor particles belong to a state of matter in the transition region between molecules and solids. Their size-dependent physical and chemical properties are currently under investigation in various fields of science. A favorite example is the well-established relationship between the optical absorption and the size of small CdS particles: with decreasing radius the onset of absorption is shifted to higher energies (size quantization effect). Other examples include their nonlinear optical properties, their unusual fluorescence behavior, their catalytic properties, their structure and phase transitions, their transport properties, their surface chemistry, and their use as precursors for nanostructured materials processing.[1-8] A key problem in these investigations is the size distribution obtained during the preparation of samples, which makes a detailed analysis of the various phenomena very difficult. Great effort has, therefore, been made to optimize the preparation conditions and to develop postpreparative size fractionation techniques. Landmarks on this road are the polyphosphate preparation of CdS,[9] the reversed micelle preparation,[10] size fractionation via exclusion chromatography,[11] gel electrophoresis,[12] and recently, size-selective precipitation of 1-thioglycerol[13] and trialkylphosphine oxide[14] stabilized particles. The latter technique allows the gram scale preparation of redispersible cluster powders with extremely narrow size distributions which can be handled like ordinary chemical substances. The final goal in this development is the synthesis and isolation of pure cluster species with a well-defined structure. So far, only a very few but remarkable examples are reported including $(Me_4N)_4[S_4Cd_{10}(SC_6H_5)_{16}]$[15] and, most recently, $Cd_{32}S_{14}(SC_6H_5)_{36}\cdot 4DMF$.[16]

This report outlines the preparation of six CdS cluster samples with extremely narrow size distributions and mean cluster diameters ranging from 13 to 39 Å obtained via size-selective precipitation. We will describe their characterization by means of UV–vis spectroscopy, X-ray diffraction, small-angle X-ray scattering, high-resolution electron microscopy (HREM), thermogravimetric analysis (TGA), and elemental analysis. We will present, for the first time, measurements of the size-dependent oscillator strength of CdS. We will show the size-dependent temperature shift of the first electronic transition in the temperature range between 4 and 295 K and discuss spectral changes between single clusters in solution and cluster solids in the form of thin transparent films.

Experimental Section

Chemicals. All chemicals used were of analytical grade or of highest purity available and obtained from Sigma, Merck, Alfa, Riedel, and Fluka.

Synthesis of the CdS Clusters. For the preparation of the CdS clusters of different sizes three methods are used:

1. Samples a–d, $2r < 20$ Å. A solution of 1.97 g (4.70 mmol) of $Cd(ClO_4)_2\cdot 6H_2O$ and 1 mL (11.53 mmol) of 1-thioglycerol in 250 mL of water was adjusted to pH 11.2 with 1 M NaOH before the addition of H_2S under vigorous stirring. The particle size was controlled by the quantity of H_2S added as well as the temperature and duration of further heating. Thus, sample b was prepared by the addition of 25 mL (1.12 mmol) of H_2S and stirring for 2 h at room temperature. In order to remove low molecular weight contaminations dialysis was carried out against water (using SERVAPOR dialysis tubings). Besides sample b the solution of the crude product also contained sample a as a byproduct. The latter could be separated by size-selective precipitation as described below. Samples c and d were prepared by the addition of 50 mL (2.23 mmol) of H_2S, heating to 100 °C for 30 min followed by stirring at 100 °C for a further 30 min. After cooling to room temperature, the crude products were also dialyzed against water and separated by size-selective precipitation.

2. Samples e and f, 20 Å $< 2r <$ 40 Å. A solution of 2.35 g (8.82 mmol) of cadmium acetate dihydrate, 0.95 g (12.48 mmol) of thiourea, and 0.95 mL (10.95 mmol) of 1-thioglycerol in 200 mL of dimethylformamide (DMF) was heated under argon flow for about 1 h. Approximately 20% (v/v) of water was added to the cooled solution, which, then, was refluxed for several hours. This procedure yielded a mixture of differently sized particles from which the clusters of sample e could be separated easily by size-selective precipitation. The larger particles of sample f were prepared by the same route but without interrupting the reaction

† University of Belgrade, Faculty of Technology and Metallurgy.
‡ Hahn-Meitner-Institut, Abteilung Solare Energetik.
* Abstract published in *Advance ACS Abstracts,* June 15, 1994.

0022-3654/94/2098-7665$04.50/0

by adding water. In this case almost monodisperse particles were obtained immediately and no size-selective precipitation had to be carried out.

3. Samples g and h, 2r > 40 Å were prepared as reference substances using the well-established polyphosphate preparation.[9] Briefly, 2 L of an aqueous solution containing 2×10^{-4} mol/L $Cd(ClO_4)_2$ and 2×10^{-4} mol/L sodium polyphosphate were purged with argon for 20 min before a stoichiometric amount of H_2S was quickly injected under vigorous stirring. The average size of the colloidal particles was determined by the pH of the solution before H_2S injection and the duration of ripening after reaction. Thus, the starting pH for sample g was adjusted to 9.4 using 0.1 M NaOH, whereas that for sample h was 5.4. The green/yellow colloidal solutions were stirred for 15 min or overnight, respectively, before the pH was increased to 11.5 to prevent further growth. The size distribution of the samples exhibited a standard deviation of approximately 15% as determined by electron microscopy.

Size-Selective Precipitation. The method of size-selective precipitation has recently been described in detail[13,14] and was used to isolate the clusters of samples a–e. Thus, the solutions of the crude products were concentrated to 25 mL using a rotary evaporator, and ethanol, 2-propanol, or acetone was added until the large particles started to precipitate. The mixtures were stirred at room temperature for at least 3 h after addition of the nonsolvent, and the supernatant and precipitate were, then, separated by centrifugation. This procedure was repeated several times until fractions of almost monodisperse crystallites were obtained. Thus, from the first preparation described above, sample b was isolated from the precipitate whereas, after successive precipitations with 2-propanol, sample a remained in the supernatant. From the second preparation, sample c was isolated from the final supernatant and sample d from the precipitate. From the third precipitation sample e was isolated from the supernatant. After isolation, all 1-thioglycerol stabilized clusters (samples a–f) were purified by reprecipitation and washing three times with alcohol or acetone and three times with diethyl ether. The precipitates were dried yielding colorless or slightly yellow powders, which could readily be redissolved in water.

UV–vis spectra were measured with an Omega 10 spectrophotometer (Bruins Instruments, Germany).

X-ray power diffraction and small-angle X-ray scattering were carried out with a Siemens D 500/5000 diffractometer operating with a Cu anode at 45 kV and 30 mA. A secondary graphite monochromator was used to select the $K_{\alpha 1}$ and $K_{\alpha 2}$ lines. The samples were prepared by finely dispersing the powders in *n*-hexane and dropping the suspensions on disorientated or silicon (100) wafers for wide-angle or small-angle scattering, respectively. After the hexane was allowed to evaporate under light shaking, plain layers of the powdered samples were obtained which were used for the diffraction experiments.

High-Resolution Electron Microscopy and Image Processing. The clusters of samples d–h were investigated with a Philips CM12 transmission electron microscope. Sample preparation was done by placing a drop of the freshly prepared cluster solution on a carbon film supported on a Cu grid. For the polyphosphate stabilized clusters (samples g and h) the mean diameter and standard deviation were determined from the obtained micrographs by averaging about 200 particles. In order to enhance the periodical and morphological information, image processing was performed with the micrographs of samples d–f. Thus, the micrographs were digitized with an Imagic Densitometer EM-1 (IMAGE-SCIENCE). According to the magnification of the microscope (550 000×) and the digitizing step (8.1 mm) the sampling distance corresponded to 0.014 nm. Representative clusters were extracted in image fields of 64 × 64 or 128 × 128 pixels, depending on the cluster size. For the analysis, 200 single particles for each sample were used. After rotation and translation alignment, classification and finally averaging were performed. This analysis was carried out with an alpha Digital DEC 3000 computer using an IMAGIC-5 software package.

Elemental analyses were carried out comercially at the microanalytic laboratory Pascher in Remagen-Bahndorf, Germany.

Thermogravimetric analyses were performed at a heating rate of 10 °C/min in the temperature interval 20–600 °C under a nitrogen flow of 20 mL/min. A Perkin-Elmer TGS-2 instrument was used. The sample masses were between 4 and 5 mg.

Absorption coefficients are referred to the analytical amount of cadmium incorporated in the clusters. Thus, aqueous stock solutions of samples a–f were prepared, and absorption spectra were taken from diluted samples. In order to convert the measured absorptions into units of the molar absorption coefficient, the cadmium concentrations were determined by polarographic means. For this, aliquots of the stock solutions were mixed with various amounts of 1 M HCl, and the concentrations of the released Cd^{2+} ions were determined with a polarographic analyzer Model 364 (EG&G, Princeton Applied Research) combined with a dropping mercury electrode. 1 M HCl was used as the supporting electrolyte. In order to test if any contaminating excess Cd^{2+} ions could be detected in the samples, polarography was also carried out at pH 9.0 where the clusters remain stable. As supporting electrolyte a 0.1 M ammonium tartrate buffer was used. These measurements revealed that no significant amounts of excess Cd^{2+} were present. In the case of the polyphosphate stabilized clusters (samples g and h), no polarographic determinations were necessary, since stoichiometric amounts of Cd^{2+} and S^{2-} were used for the preparation and almost 100% conversion is to be expected. Thus, in this case, the overall amount of $Cd(ClO_4)_2$ used for preparation was taken to calculate the absorption coefficients.

Temperature-dependent Absorbance Shift. For temperature-dependent measurements the 1-thioglycerol stabilized clusters were prepared as fully transparent thin films on quartz plates by spin coating from the concentrated solutions using a convac spin coater, Model 146/1001. Two or three drops of the solution were placed in the center of the quartz plate which was then spun at 1000 rpm for 90 s after a build-up time of 9 s to 1000 rpm. The required optical density was obtained by adjusting the concentration of the solution and/or the number of layers applied. Approximately, the optical density, and hence the film thickness, increased proportionally to the number of applied layers. The absorption spectra of these films were measured with an Omega 20 spectrophotometer (Bruins) equipped with a Leybold VKS 4-300 helium flow cryostate in the temperature range from 4 to 295 K.

Results

Synthesis of the Clusters. Figure 1a shows a set of spectra recorded during the preparation of samples a and b. The maximum at 292 nm (spectrum 3) can be clearly seen only after ripening of the clusters in the dialysis tubes. Moreover, it is recognized that the long wavelength tail of absorption spectrum 1 recorded immediately after H_2S injection decreases with time.

Figure 1b shows a set of absorption spectra which were recorded during a typical synthesis of samples c and d after various times of heating after H_2S injection. During the first 5 min the formation of an absorption band around 280 nm is seen (spectrum 1). With increasing heating time, i.e., with successive cluster growth, this band disappears and a new band rises at 308 nm (spectrum 2) which then again decreases and a new band at 333 nm appears (spectra 3 and 4). Thus, during the cluster growth, these maxima did not shift gradually but one absorption band was formed at the expense of another. This type of spectral development was observed for all 1-thioglycerol stabilized clusters. The peak position of the absorption bands varied only very slightly (±2 nm) from one run to another.

The spectra obtained during the growth of the clusters in DMF are plotted in Figure 1c. Again the development of larger clusters

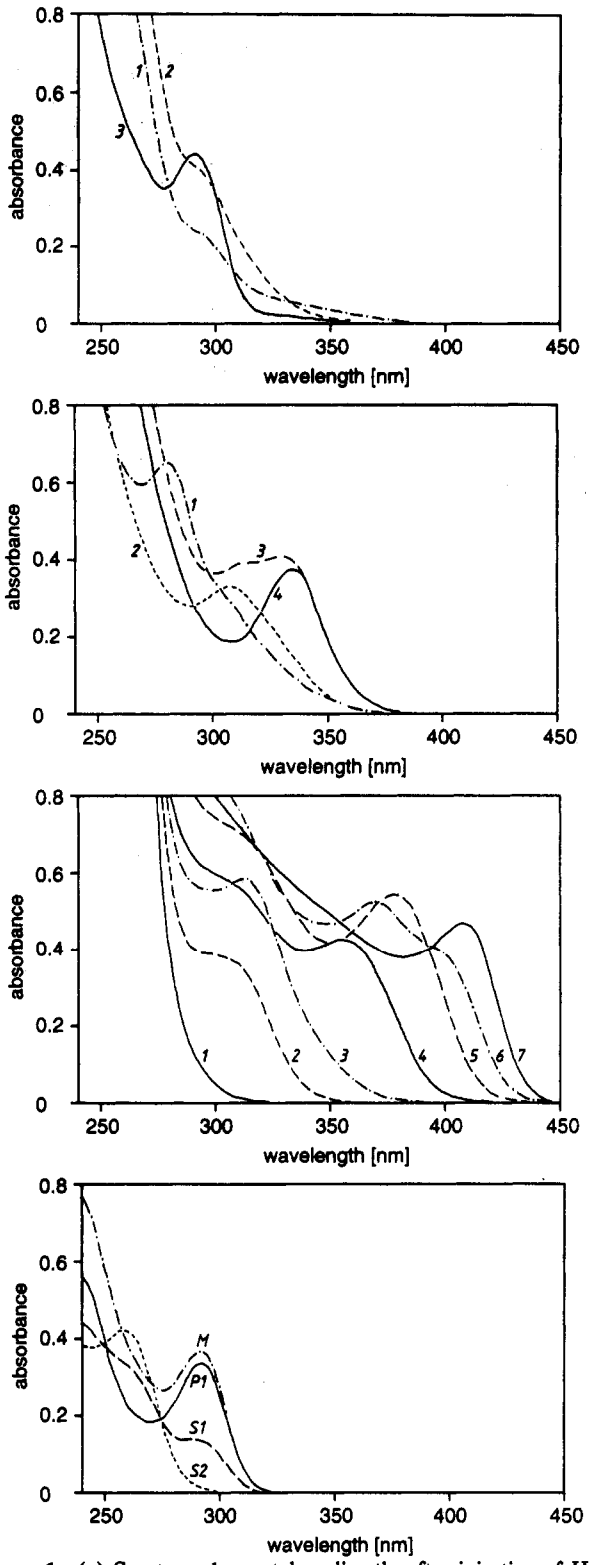

Figure 1. (a) Spectrum 1 was taken directly after injection of H_2S. Spectrum 2 was taken after stirring for 2 h at room temperature, and spectrum 3 represents the mixture obtained after dialysis from which samples a and b were separated. (b) Spectra 1–4 were taken during the course of prolgoned heating after H_2S injection. Sample c was isolated from the mixture represented by spectrum 3, whereas sample d could be isolated from the mixtures represented by spectra 3 and 4. (c) Spectrum 1 shows the reaction mixture in DMF before heating. Spectra 2–5 were taken after different times of heating. Spectrum 6 was taken after addition of water and further heating. This mixture leads finally to sample e. Spectrum 7 was recorded after prolonged heating without adding water. This route leads directly to a solution of pure sample f. (d) Spectrum M represents the mixture from which samples a and b were separated. After the first precipitation spectrum S1 was taken from the supernatant containing both samples a and b. Spectrum P1 represents the redissolved precipitate which is almost pure sample b. After the second precipitation sample a was obtained in the supernatant as represented by spectrum S2.

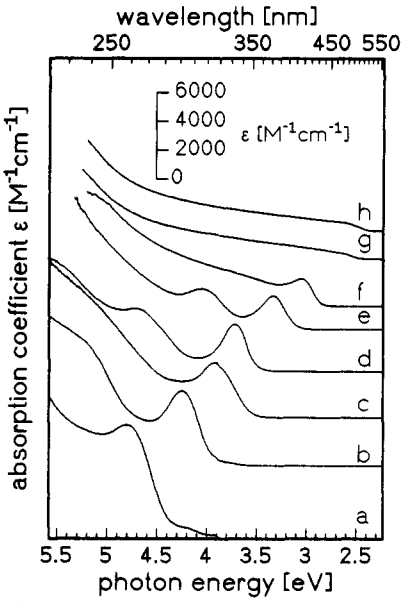

Figure 2. UV–vis spectra of the isolated clusters. Note that with decreasing cluster size the excitonic transition is shifted toward higher energies and the molar absorption coefficient, which refers to the concentration of Cd, increases.

TABLE 1: Comparison of Size, Excitonic Transition Energy, Oscillator Strength, and Composition of the Investigated Clusters

sample	cluster radius,[a] Å	E_g[c] eV (nm)	oscillator strength f/f_{ex}[d]	elemental analysis, mass % Cd/C/H/O/S	Σ
a	6.4	4.78 (259)	57.5	34.0/21.2/4.2/21.7/18.9	100.0
b	7.2	4.22 (294)	27.9	38.8/20.1/4.1/17.2/19.0	99.2
c	8.0	3.89 (319)	22.3	39.0/20.1/4.1/17.2/19.0	99.4
d	9.3 (10)[b]	3.72 (334)	12.2	45.6/14.8/3.0/13.8/19.8	97.0
e	11.6 (13)[b]	3.32 (373)	8.7	48.1/15.2/2.9/11.8/20.8	98.8
f	19.4 (22)[b]	3.05 (407)	6.1	56.9/10.4/2.1/7.5/22.1	99.0
g	28[b]	2.68 (462)	2.7		
h	48[b]	2.60 (476)	3.9		

[a] By small-angle X-ray scattering. [b] By electron microscopy. [c] From UV–vis spectra using the minimum of the second derivative. [d] Referred to the analytic amount of Cd and normalized with f_{ex} = 0.00256.[18]

at the expense of smaller ones is seen, but it should be mentioned that the growth of the clusters seems to become more and more continuous with increasing size. Thus, absorption bands at wavelengths longer than about 390 nm were shifted continuously toward lower energies upon further heating of the solution. This preparation route leads straightforwardly to sample f (spectrum 7), whereas sample e was separated from a mixture, which was obtained after addition of water and further heating (spectrum 6).

To visualize the process of size-selective precipitation, four spectra obtained during the separation of samples a and b are shown in Figure 1d. One clearly sees that after the first precipitation, pure sample b was obtained in precipitate P1 while sample a in supernatant S1 was still contaminated with the larger clusters of sample b. After the second precipitation pure sample a was obtained in supernatant S2.

UV–Vis Spectra. Figure 2 shows the absorption spectra of the isolated cluster samples a–f and, for comparison, the spectra of the polyphosphate stabilized samples g and h. The most striking features are as follows: first, all the 1-thioglycerol stabilized particles (a–f) show a well-developed maximum near the onset of absorption which is ascribed to the first excitonic (1s–1s) transition. In some cases even higher energy transitions are observed. Second, with decreasing particle size the transition energies shift to higher values as a consequence of the size quantization effect (see also Table 1). Third, the integrated absorption coefficients also increase enormously with decreasing particle size. These properties will be investigated in detail below.

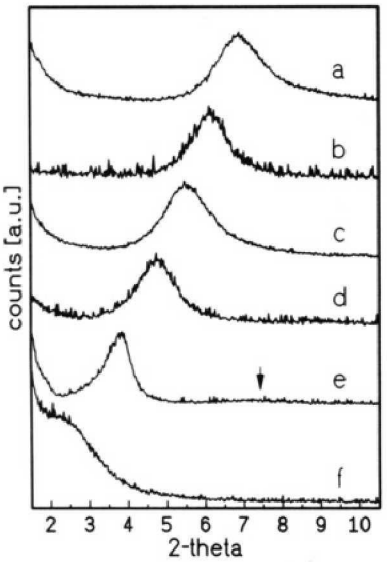

Figure 3. Small-angle powder X-ray diffractograms of the 1-thioglycerol stabilized samples. The arrow indicats the second-order reflex of sample e.

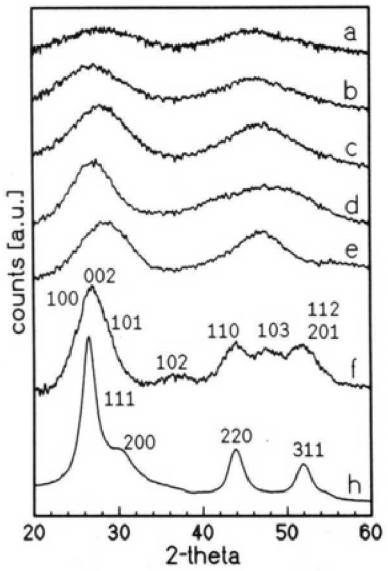

Figure 4. Wide-angle powder X-ray diffractograms of the 1-thioglycerol stabilized samples a–f and the polyphosphate stabilized sample h. The hexagonal diffraction pattern of sample f is clearly seen, whereas the larger clusters of sample h display a cubic pattern. For the latter two the *hkl* indices are given.

Powder X-ray Diffractograms and Cluster Sizes. In order to determine the mean cluster size, we examined small-angle X-ray diffraction on the powdered samples (Figure 3). Samples a–e show sharp diffraction peaks between $2\Theta = 7.5°$ and $2\Theta = 3.5°$, whereas sample f displays a shoulder around $2\Theta = 2.5°$. The peak angle maxima can be converted to the nearest neighbor distances of the clusters in the powdered samples by using the Bragg equation. These distances were used as a measure of the mean particle size (including the ligands). In the case of sample e a weak shoulder is also seen around $2\Theta = 7.5°$, i.e., at the double angle of the main diffraction peak. The particle sizes determined from the small angle diffraction peaks are listed in Table 1.

Figure 4 shows the wide-angle X-ray diffraction pattern of samples a–f and of sample h for a comparison. Due to the small particle size the diffractograms of samples a–e exhibit only very broad diffraction peaks from which a clear identification of the crystalline structure is, obviously, not possible. However, in the case of samples f and h, which contain larger particles, the crystalline structure is readily derived from the diffractograms. The result is astonishing: the 1-thioglycerol stabilized clusters

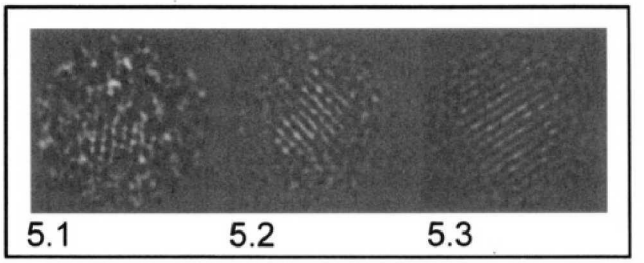

Figure 5. TEM images of the three cluster samples d, e, and f labeled 5.1, 5.2, and 5.3, respectively; for details see text.

of sample f are clearly hexagonal (wurtzite phase) whereas the larger polyphosphate stabilized particles are clearly cubic (zincblende phase).

Electron Microscopy. In order to further elucidate the size, shape, and crystal structure of the clusters, HREM images were taken. Overivew images do not provide much information other than the particles are uniform in size and tend to agglomerate. We also found that the microscope images had to be taken at the lowest electron beam doses as, otherwise, the clusters coalesced into larger particles. We, therefore, investigated only areas where individual clusters could clearly be identified. Those were usually found on the TEM grids close to areas of agglomerated clusters, and we convinced ourselves that we investigated representative clusters. Figure 5 shows a gallery of single clusters of samples d (Figure 5.1), e (Figure 5.2), and f (Figure 5.3). The images were obtained after signal averaging over 200 clusters (see Experimental Section). For the smallest clusters considered here (sample d) it is rather difficult to reliably determine the shape, but in the case of sample e one recognizes an edged, pyramidal geometry. The shape of the larger clusters of sample f resembles an ellipsoid. All images in Figure 5 exhibit an interplanar distance of 3.4 Å which is observed in the cubic ((100) planes) as well as in the hexagonal ((002) planes) phases. However, in the case of samples d and e we also observed particles displaying the characteristic spacing of 2.9 Å for the (200) planes of the cubic phase. In the case of sample f those distances could not be observed, but instead, lattice plane spacings of 3.6 Å were detected characteristic of the (100) planes of the hexagonal phase.

From Figure 5, the size of the clusters can be estimated by counting the number of lattice planes. We recognize approximately 6, 8, and 13 contrasting lattice planes corresponding to particle radii of 10, 13, and 22 Å for samples d, e, and f, respectively. These values are also listed in Table 1 together with the radii obtained by small-angle X-ray scattering.

Elemental Analysis. To investigate the elemental composition of the 1-thioglycerol stabilized clusters, we carried out elemental analyses with the purified samples. Table 1 presents the results given in mass %. For each sample the summation of all determined elements approximates 100% meaning that other elements are not present in significant amounts. From the analysis, the stoichiometric ratios of S (suflur which is not bound to an organic residue) to Cd and RS (1-thioglycerol) to Cd for each cluster can easily be obtained. The results are visualized in Figure 6. Herein, the portion of 1-thioglycerol was based on the analysis of carbon, but it should be mentioned that the stoichiometric ratio of C/O/H agrees well with the stoichiometry of 1-thioglycerol in all cases. It is recognized that the relative amount of 1-thioglycerol decreases steadily with increasing cluster size, whereas the amount of sulfur, which is not bound to an organic residue, increases relative to that of cadmium. Besides that, it is noteworthy that the relative stoichiometry of Cd, S, and RS, as well as the fact that no other elements are present in significant amounts, reveals that the clusters are not highly charged and possibly even uncharged.

Thermogravimetric Analysis. In order to confirm the stoichiometry derived from elemental analysis, thermogravimetric analysis of the 1-thioglycerol stabilized clusters was performed.

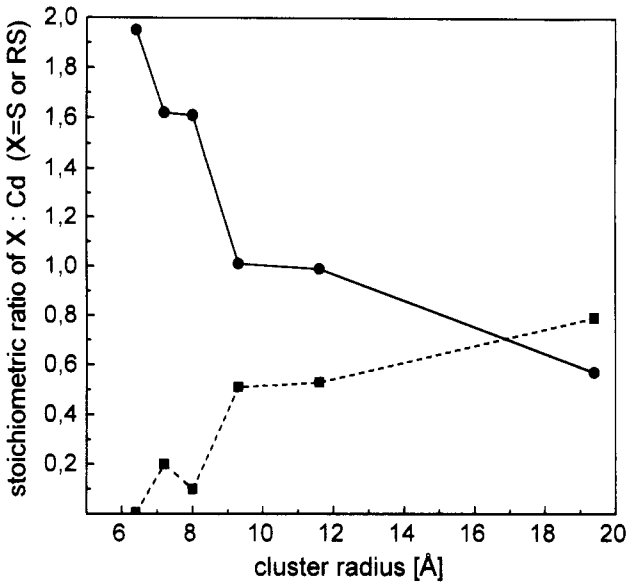

Figure 6. Relative stoichiometric composition as a function of the cluster size for all 1-thioglycerol stabilized samples (a–f). The ratio RS/Cd (●) decreases with increasing size, while the ratio S/Cd (■) increases. The portion of RS was calculated based on the analysis of carbon.

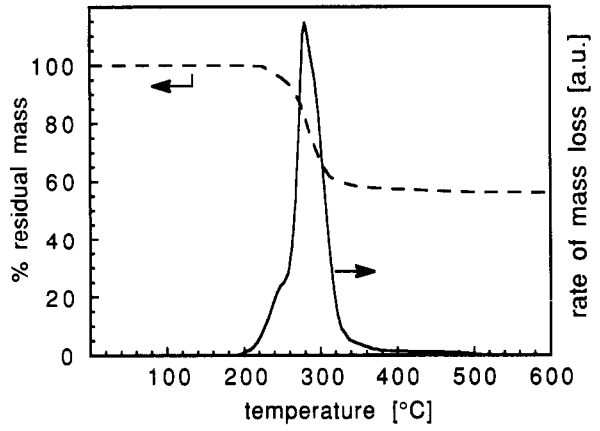

Figure 7. Thermogravimetric analysis of sample b. The upper part shows the % residual mass, whereas in the lower part the corresponding derivative curve is seen. Three decomposition peaks can be distinguished.

A typical example is shown in the upper part of Figure 7 for sample b (dashed line). A mass loss of 44% is seen in the temperature range between 250 and 300 °C. From the lower part of the figure, where the derivative curve is depicted (solid line), it is readily seen that mass loss does not occur in one step but that several processes are involved. At least three different decomposition peaks can be extracted from the derivative thermogravimetric (TG) curve. For all cluster samples the TG curves were very similar. The total mass loss from TGA is plotted in Figure 8 versus cluster size, and as can be seen, it decreases with increasing cluster size. It is most likely that the mass loss is mainly caused by the decomposition of the organic ligand in the course of which the Cd–SR and/or the CdS–R bonds are cleaved. For comparison, we calculated three possibilities by using the results of the elemental analysis: first, it was assumed that all the 1-thioglycerol is stripped off the samples, meaning that the Cd–SR bonds are cleaved. Second, Cd–SR bonds as well as CdS–R bonds are cleaved and a stoichiometric amount of pure CdS is left as a residue. Third, the CdS–R bonds are cleaved and only carbon, oxygen, and hydrogen are stripped off the samples. The latter assumption showed quantitatively the best agreement with the TG results, but in all cases the same trend agreeing with the TGA results can be seen: with increasing cluster size a decrease in the mass loss is to be expected. In this context it should be mentioned that the color of the residues obtained after TGA was not pure yellow but slightly brown or

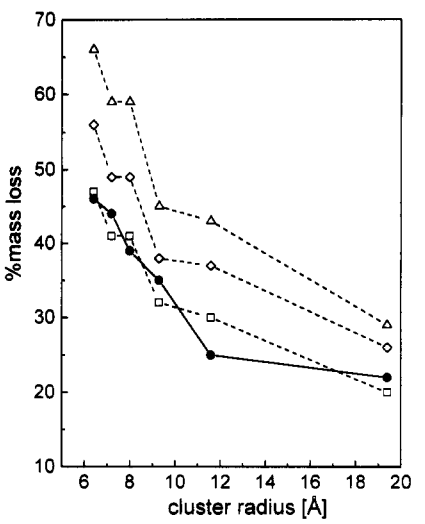

Figure 8. TGA results compared with values obtained from elemental analysis. ●, results of TGA; △, mass % of RS; ◇, mass % of C, H, O, and partly S, so that pure CdS would be obtained as residue; □, mass % of C, H, and O. The latter three were calculated using the results of the elemental analysis.

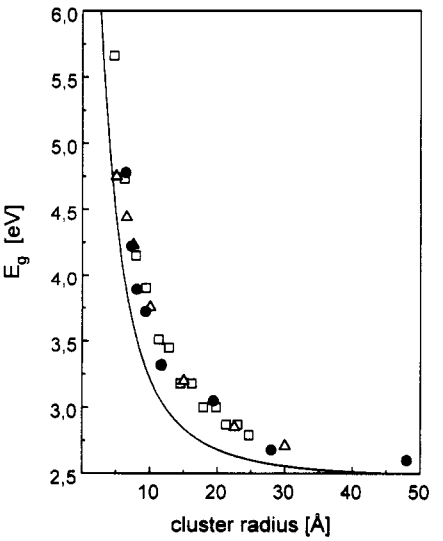

Figure 9. Size quantization effect: the energy of the first electronic transition increases with decreasing particle size. The experimental data points (●) are compared with values obtained from the tight-binding (□) and pseudopotential (△) theories. The fit was calculated using a finite depth potential well model.

black depending on the cluster size, meaning that traces of decomposed material remained as well as CdS.

After having characterized the cluster samples as described above, some optical properties were investigated in more detail:

Size Quantization Effect and Oscillator Strength. As mentioned before, Figure 2 shows clearly that the electronic transition energies are shifted toward higher energies with decreasing cluster size. This so-called size quantization effect is also visualized in Figure 9. The respective values were taken from Table 1 and are compared with theoretical considerations (see Discussion).

Besides the size quantization effect, Figure 2 also reveals that the extinction coefficients of the first excitonic transition become much larger with decreasing cluster size. In this figure, the absorption coefficients refer of the analytical concentration of cadmium (as outlined in the Experimental Section) and not to the respective whole clusters. This was done since so far the exact agglomeration number of the clusters cannot be given. The oscillator strength f (also based on the analytical amount of cadmium) is readily obtained according to[17]

$$f = 4.32 \times 10^{-9} \times \mathcal{A}$$

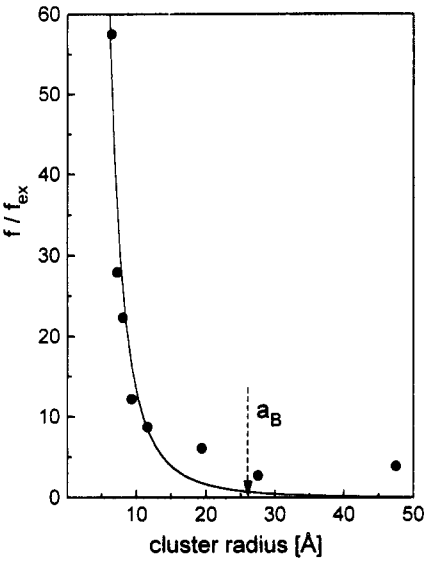

Figure 10. Normalized oscillator strength of the first excitonic transition referred to the analytical amount of Cd as a function of the cluster size. The data are also shown in Table 1. The data points are compared with a fit using a theoretical model which is valid for the strong confinement region ($r < a_B$); for details see text.

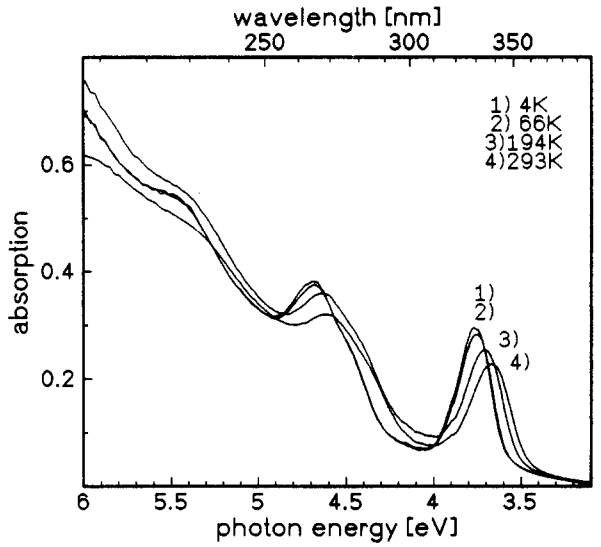

Figure 11. UV spectra of sample d as a film on a quartz plate at four different temperatures. With decreasing temperature the spectra are shifted toward higher energies and the bands become sharper, whereas the oscillator strength of the 1s–1s transition remains constant.

where $\mathcal{A}$ is the integrated absorption coefficient referring to the wavenumber scale. $\mathcal{A}$ was taken from Figure 2 by doubling the area of the low-energy half of the 1s–1s transition band and transferring the obtained values to the wavenumber scale. For the large, polyphosphate stabilized clusters (samples g and h) $\mathcal{A}$ was determined from the area of a Gaussian function fitting the onset of absorption. Figure 10 shows the obtained oscillator strengths related to the value of the free exciton in bulk CdS (f_{ex} = 0.002 56)[18] as a function of the cluster radii.

Low-Temperature Absorption Measurements. Figure 11 shows the absorption spectra of sample d at four different temperatures. With decreasing temperature the 1s–1s transition energy shifts by about 100 meV toward higher energies and the bands become sharper. The band area, which is proportional to the oscillator strength, does not change with temperature as expected for an allowed optical transition. This observation was made for all 1-thioglycerol stabilized particles. The data points of the temperature-dependent energy shift of the 1s–1s transition are shown in Figure 12. It can be seen as a trend that the temperature dependence becomes stronger with decreasing cluster size. For

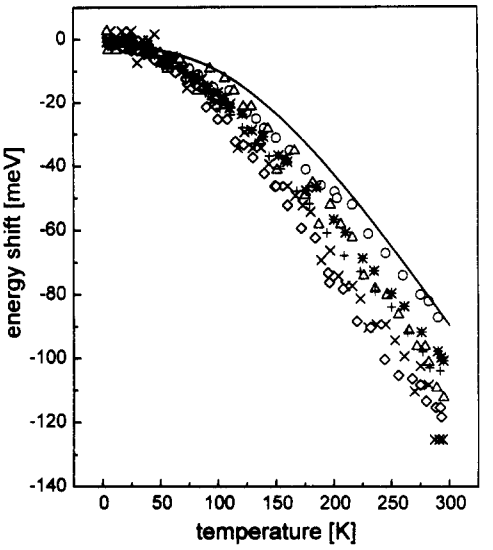

Figure 12. Temperature-dependent shift of the first excitonic transition for all 1-thioglycerol stabilized samples (×, a; △, b; ◇, c; +, d; *, e; ○, f). The temperature dependence becomes steeper with decreasing particle size. The data points are compared with a fit using a theoretical model for bulk CdS; for details see text.

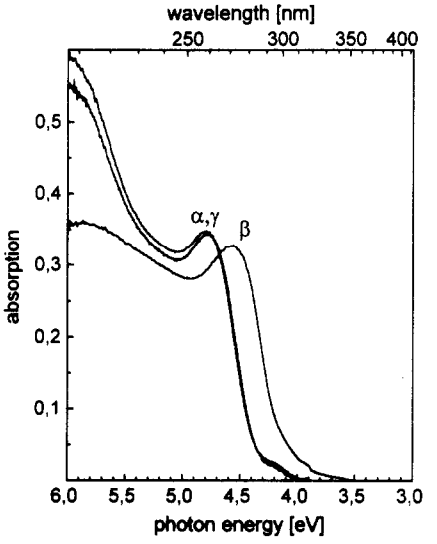

Figure 13. Reversible absorbance shfit comparing a film and a solution prepared from sample a. Spectrum α was taken from a solution in water, spectrum β as a film on quartz, and spectrum γ after redissolving the film in water.

the largest particles (sample f), the slope of the linear temperature shift above 150 K was determined to be –0.40 meV/K. This value increases gradually with decreasing particle size and reaches –0.55 meV/K for the smallest cluster (sample a). As a consequence, the maximal energy shift in the considered temperature region is up to about 40 meV larger for the smaller particles than for the largest. In the region below 50 K a linear temperature shift with a slope of around –0.1 meV/K was determined for all samples.

Reversible Absorbance Shifts. During the preparation of the transparent cluster films for low-temperature measurements a remarkable observation was made: The spectral position of the 1s–1s absorption band varied reversibly between solution and cluster film. This can be seen very clearly in Figure 13. Spectrum α was taken with sample a in solution. The film formed from this solution exhibits spectrum β, which is shifted by about 250 meV to lower photon energies. The film could readily be redissolved yielding spectrum γ which is, obviously, identical with the spectrum of the original cluster solution. For the larger clusters, this shift became much smaller varying between 0 and 50 meV.

Discussion

In colloid chemistry, particle growth usually occurs via the mechanism of Ostwald ripening, i.e., larger particles grow on account of dissolution of smaller ones. As a result, the particle size increases continuously during growth. Since the size of the particles is directly related to the absorption wavelength of quantum sized particles, Ostwald ripening is recognized as a continuous shift of the excitonic absorption band to longer wavelengths. In the case of the 1-thioglycerol stabilized CdS clusters this type of spectral development was only observed if a certain cluster size was exceeded. Thus, during the preparation of sample f the excitonic absorption band shifted continuously to longer wavelengths after exceeding approximately 390 nm. In the case of all smaller clusters, i.e., those with excitonic absorption bands below 390 nm, growth did not occur via Ostwald ripening. Instead, discontinuous cluster growth was observed, reflected by the occurrence of well-defined absorption maxima appearing reproducibly always at the same wavelengths (see Figure 1 parts a–c). Very similar behavior was found several years ago for the growth of very small polyphosphate stabilized CdS particles in aqueous solution.[11] At that time it had been proven by exclusion chromatography experiments that these clusters also grow discontinuously until they have reached a certain size and Ostwald ripening starts to determine the growth mechanism. The formation of small CdS clusters with certain agglomeration numbers might have two reasons: particle growth proceeds via coalescence, i.e., two small clusters fuse to form a larger one, or clusters of well-defined structures are thermodynamically more favorable than others. If one compares cluster sizes and excitonic transition energies (see Table 1) with the positions of the absorption bands observed during sample preparations (Figure 1 parts a–c), one must conclude that the differences in size between the observed intermediate species are too small to agree with a simple coalescence mechanism. On the other hand, Figure 1a shows that the long wavelength tail of absorption spectrum 1 decreases in magnitude on standing at room temperature while the absorption at 292 nm increases. This observation suggests that the larger clusters responsible for the tail are formed during the fast reaction with H_2S and that they are subsequently converted into smaller but thermodynamically more favored ones. Thus, we regard the formation of the small 1-thioglycerol stabilized CdS species (samples a–e) as a result of thermodynamically controlled cluster growth. However, in this context it should be noted that Wang and co-workers claimed fusion of two $[Cd_{10}S_4(SC_6H_5)_{16}]^{4-}$ clusters under formation of $[Cd_{20}S_{13}(SC_6H_5)_{22}]^{8-}$.[3]

In this paper we showed that small-angle X-ray scattering can easily be used to determine the sizes of the small clusters (see Figure 3 and Table 1, samples a–e). This has also been observed previously by Dameron et al., who investigated small, biogenic, short-peptide-capped CdS clusters.[19] The fact that low-angle diffraction peaks which reflect the nearest neighbor distances can be observed (in the case of sample e even a second-order peak is seen) reveals that the prepared samples contain almost monodisperse clusters. The advantage of using these peaks for size determination is that one averages over a macroscopic amount of clusters. Moreover, it is especially advantageous for extremely small clusters as those of samples a–c which are, due to the diminishing contrast, hard to detect by electron microscopy.

As mentioned in the Results section, the wide-angle X-ray diffraction pattern of sample f (Figure 4) reveals a hexagonal lattice structure whereas sample h was found to be cubic. A reason for this remarkable observation might the the fact that two different stabilizers have been used, namely 1-thioglycerol and sodium polyphosphate, respectively. It also has to be taken into account, however, that the preparation routes for both samples are quite different: the 1-thioglycerol stabilized clusters of sample f were synthesized by refluxing the reaction mixture for some hours in DMF whereas the polyphosphate stabilized clusters of sample h were prepared under much milder conditions, i.e., the reaction was carried out at room temperature in aqueous solution without heating. It should be mentioned in this context that room temperature synthesis of CdS nanoparticles mostly yields the cubic phase,[20] whereas CdS particles in the hexagonal phase were obtained only when high temperatures were applied during preparation.[14] Since bulk CdS is almost exclusively found in the thermodynamically favored hexagonal phase it is concluded that the polyphosphate stabilized clusters of sample h were obtained under kinetic control, whereas the 1-thioglycerol stabilized clusters of sample f were formed under thermodynamic control.

Clear conclusions about the crystalline phase of samples a–e cannot be drawn from diffractograms, since the clusters are very small and display only very broad diffraction peaks. In the case of samples d and e, we tried to fit the diffraction pattern as a sum of Lorentzians fixing only the peak maxima corresponding to the bulk values. None of the diffractograms could be fitted reasonably irrespective of whether parameters for the cubic or hexagonal phase were used.

The results from our electron microscopy investigation on sample f are consistent with our results obtained by wide-angle X-ray diffraction since the lattice plane spacing of 3.6 Å was detected, which is typical for the hexagonal phase. On the other hand, the clusters of samples d and e both exhibited lattice plane distances of 2.9 Å which are found only in the cubic phase. As already speculated above, this result reveals that not only the choice of the ligand but also the route of preparation determines the lattice structure.

The cluster sizes determined by electron microscopy and small-angle X-ray scattering are in good agreement (see Table 1). However, it is noticed that in each case the size determined by TEM is slightly larger, although the opposite should be expected since TEM does not take into account the covering ligand. In this context, it should be mentioned that the method of image processing might lead to confusion because it is not possible to obtain a perfect superposition of the 200 clusters used for averaging. Thus, lattice planes might be added by mistake at the edges of the cluster. Although such planes will be of low contrast they might fake a larger cluster size that would explain the observed differences. Moreover, the shape of the clusters could also influence differently the results obtained by both methods. Although it is not possible to elucidate the cluster's shape in the case of sample d by electron microscopy (Figure 5.1) an edged shape is seen in the case of sample e (Figure 5.2), which might reflect the surface of a tetrahedral geometry. This could mean that the clusters of this sample might be larger members of the same families as the tetrahedral clusters $[S_4Cd_{10}(SC_6H_5)_{16}]^{4-}$ or $[S_4Cd_{17}(SC_6H_5)_{28}]^{2-}$ and $S_{14}Cd_{32}(SC_6H_5)_{36}\cdot 4DMF$ discovered by Dance and co-workers[15,21] and Wang and coworkers.[16] However, in the case of sample f (Figure 5.3) we observe an ellipsoidal shape. Taken together, the shape of the clusters can not be considered to be simply spherical but might be edged and possibly oblong. Such an oblong shape would also hold for the size differences observed with both methods, since the small-angle X-ray peaks might be due to two-dimensional aggregates and thus reflect only the nearest neighbor distance in one direction, whereas we possibly count the number of lattice planes in another direction in the TEM images.

It should also be mentioned that the single clusters observed on the grids typically varied in the number of lattice planes by ±1. It cannot be expected that the very first lattice "planes" at the edges of a pyramidal oblong structure can reliably be detected in the images. Thus, the variation of the number of detected lattice planes is not necessarily due to size fluctuation but lies with the limitations of such HREM investigations. Therefore, we do not want to give numbers for the size distributions in our samples. Especially because samples d and e appear to monodisperse that deviations in "size" are more probably due to "molecular " defects, e.g., a missing edge at a tetrahedron or

steps at the surface planes, than to typical size fluctuations as in the case of the larger colloids (as in samples g and h).

Our results obtained by elemental analysis reveal that with increasing cluster size the ratio RS:Cd decreases whereas S:Cd increases (Figure 6). This is expected since the surface to volume ratio decreases with increasing cluster size. Thus, with increasing cluster size the relative portion of RS which covers the surface must decrease and the amount of S which is located in the core of the particle must increase. The most remarkable result is that the stoichiometry of Cd^{2+}, S^{2-}, and RS^- for each cluster reveals that these compounds are not highly charged and possibly even uncharged. The stoichiometry found in the case of sample a, which does not contain any core S, would agree with the formula $Cd_{10}(SCH_2CH(OH)CH_2OH)_{20}$. This suggests that we might have synthesized a cluster which resembles a structure determined by Strickler for $Cd_{10}(SCH_2CH_2OH)_{16}^{4+}$.[22] This structure was found as a portion of the cubic CdS lattice in which four Cd atoms at the vertices form a tetrahedron. Since these Cd atoms are coordinated by only three sulfur atoms they tend to coordiante with one more RS^-, thus forming $Cd_{10}(SCH_2CH_2OH)_{20}$[23]; perhaps this is what happened in the case of our sample a. However, as described by Dance and co-workers there exist a number of different CdS cluster families[15,21,24] and one can only speculate that, for example, the clusters of sample b could be of the type $[S_4Cd_{17}(SR)_{28}]^{2-}$. Since we do not know the exact agglomeration numbers for the 1-thioglycerol stabilized clusters, we do not want to make further suggestions concerning the structure and formula so far.

The results obtained by TGA reveal that at least three different decomposition steps are passed while heating the samples (Figure 7). This might reflect the occurrence of different bonded RS ligands, namely, μ_3-, μ_2-, and terminating RS groups. Figure 8 suggests that during the decomposition the CdS–R bonds are cleaved, and one can imagine that the strength of these bonds depends on how the sulfur is bound to the cadmium atoms.

The size quantization effect, which is noticed as a shift of the transition energies toward higher values with decreasing particle size, is still a subject of great theoretical interest. In Figure 9 we compared our experimental values of the first electronic transition energies with pseudopotential calculations by Rama Krishna and Friesner[25] (referred to the hexagonal crystal structure and taking into account the lattice contraction) and with results of the tight-binding theory of Lippens and Lannoo[26] (using their calculated band gap energies referred to the cubic crystal structure). As seen, in both cases we found very good agreement between theory and the experimentally obtained results. On the other hand we compared our results with a calculation using a finite depth potential well model which is described in detail in ref 27. Obviously, this model does not work showing that an effective mass approximation is not sufficient for the small clusters considered here. However, although the pseudopotential and the tight-binding theory describe the observed behavior well, it should be kept in mind that the mean cluster sizes (samples a–f) were determined by small-angle X-ray scattering, a method which not only takes into account the CdS core but also the stabilizing ligand. Thus, subtracting approximately 2 Å in radius to account for the ligand, the finite depth potential well model mentioned above would be in better agreement with the results for samples a–e.

Besides the size quantization effect the size dependent oscillator strength of the first excitonic transition is of great theoretical interest. In the strong confinement region ($r <$ excitonic Bohr radius a_B) the oscillator strength is expected to increase with $1/r^3$ because of the strong overlapping of the wave functions of the confined electron and hole. For spherical particles this can be expressed as[28]

$$\frac{f}{f_{ex}} \approx \frac{3}{4}\left(\frac{a_B}{r}\right)^3$$

where f_{ex} is the oscillator strength of the exciton in the bulk material per CdS unit (i.e., $f_{ex} = 0.002\,56$) and $a_B = 26$ Å. This function is plotted in Figure 10 together with the experimentally obtained values. One clearly observes good agreement between experiment and theory for clusters smaller than 15 Å in radius. It is noted that this result is also in agreement with the prediction that the oscillator strength per cluster is independent of the cluster size within the strong confinement region.[29] Recently, Rajh et al.[30] obtained the same results by determining the oscillator strengths of CdTe particles. In contrast to this study, their conclusions were derived from samples with rather broad size distributions.

The temperature dependence of the first electronic transition energy of bulk CdS has been successfully described using the Radkowsky–Fan relation and taking into account the crystal dilation and piezo electric scattering:[31-34]

$$\Delta E_g = -\frac{\pi(ee^*)^2}{a^3 M}\left(\frac{2m_e}{\hbar\omega^3}\right)^{1/2}((m_h^*)^{1/2} + (m_e^*)^{1/2})\frac{\exp(\hbar\omega/kT)}{\exp(\hbar\omega/kT)-1} + c_1 T + c_2 T$$

where $e^* = 0.72e$ is the effective charge on the electron, $a = 2.91 \times 10^{-8}$ cm is the interionic distance, $M = 4.14 \times 10^{-23}$ g is the reduced mass of the two ions, $\omega = 5.8 \times 10^{13}$ s^{-1} is the frequency of the longitudinal optical (LO) phonon, $m_e^* = 0.208$ and $m_h^* = 0.984$ are the effective masses of the electron and the hole (allowing for the anisotropy of hexagonal CdS), the constants $c_1 = -2.5 \times 10^{-5}$ eV/K and $c_2 = -4.9 \times 10^{-5}$ eV/K take into account the crystal dilation and the piezo electric scattering, respectively. This equation was used to create the fit shown in Figure 12 which was also corrected for the zero-temperature shift to allow a direct comparison between theory and experiment. Although our largest 1-thioglycerol stabilized clusters (sample f) were much smaller than the dimensions of the bulk exciton, we found reasonable accordance for this sample without altering any parameter. However, by decreasing the cluster size the temperature dependence became significantly steeper and did not obey this equation anymore. Considering the equation, this might suggest that with decreasing cluster size the effective masses of the charge carriers increase. On the other hand, a size dependency of the LO phonon frequency could also alter the slope of the curves. This effect has been discussed controvertibly. Indeed, for CdSe crystallites a decrease of the LO phonon frequency with decreasing particle size has been observed[35] and this would agree with our observations. In another report, however, no size dependence of the LO phonon frequency could be observed for small CdS particles with radii as low as 10 Å.[36] It is mentioned that size-dependent contributions of low-frequency acoustic phonons may also be important for the observed behavior. For 22-Å CdSe clusters it has been shown that acoustic phonon coupling accounts for roughly half of the homogeneous line width even at low temperatures.[37] Besides this, changes of the linear terms should be expected by decreasing the particle size and ending up with molecule like compounds. While the structure of the largest 1-thioglycerol cluster (sample f) was determined to be hexagonal, the lattice of all other 1-thioglycerol stabilized samples seemed to be neither hexagonal nor cubic, probably due to stacking faults. For this reason both the piezo electric scattering and the effective masses of the charge carriers should be different.

As shown in many studies including this one, the transition from molecules to solids in quantum-sized semiconductor particles is accompanied by a series of interesting properties which are based on the varying electronic structure of the individual nanoclusters with size. Very similar effects should be observed if, instead of adding atom to atom (or molecule to molecule), bulk solids are built up by packing cluster by cluster into a three-dimensional framework. The reason why this highly interesting field of science has been strongly neglected so far is simply of experimental nature. As a prerequisite for clusters to form

collective electronic modes similar to the energy bands of conventional bulk semiconductors, the clusters must be very homogeneous in size and the intercluster distance must be on the order of few angstroms. The conditions are probably fulfilled in the spin-coated cluster films. Therefore, it appears plausible to understand the reversible absorbance changes between cluster solution and cluster film (Figure 13) in terms of cluster–cluster interaction in the films, resulting in collective excitation modes. One should, however, keep in mind that the optical transition in the small clusters is shifted so strongly to higher photon energies that the photoexcited electron must be in a state close to the ionization threshold. In this size regime the nature of the optical transition should, gradually, change from excitonic excitations to charge-transfer transitions. Thus, a change of the chemical environment/solvent should strongly influence the spectral position of the absorption band, as it is known to occur in molecular photochemistry. In order to distinguish between solvation effects due to changes of the dielectric environment and collective excitation modes we are currently performing investigations of electron transport properties in the films as well as photoionization experiments. Details will be reported in a forthcoming paper.

Acknowledgment. Thanks are due to Mrs. U. Bloeck for her skillful work at the electron microscope, and to Mr. A. Kornowski, Mr. A. Mews for their helpful contributions concerning the characterization of the polyphosphate stabilized CdS clusters.

References and Notes

(1) Brus, L. E. *Appl. Phys. A* **1991**, *53*, 465.
(2) Henglein, A. *Chem. Rev.* **1989**, *89*, 1861.
(3) Wang, Y.; Herron, N. *J. Phys. Chem.* **1991**, *95*, 525.
(4) Weller, H. *Angew. Chem., Int. Ed. Engl.* **1993**, *32*, 41.
(5) Weller, H. *Adv. Mater.* **1993**, *5*, 88.
(6) Tolbert, S. H.; Alivisatos, A. P. *Z. Phys. D* **1993**, *26*, 56.
(7) Goldstein, A. N.; Echer, C. M.; Alivisatos, A. P. *Science* **1992**, *256*, 1425.
(8) Chemseddine, A. *Chem. Phys. Lett.* **1993**, *216*, 265.
(9) Spanhel, L.; Haase, M.; Weller, H.; Henglein, A. *J. Am. Chem. Soc.* **1987**, *109*, 5649.
(10) Fendler, J. H. *Chem. Rev.* **1987**, *87*, 877.
(11) Fischer, C.-H.; Weller, H.; Katsikas, L.; Henglein, A. *Langmuir* **1989**, *5*, 429.
(12) Eychmüller, A.; Katsikas, L.; Weller, H. *Langmuir* **1990**, *6*, 1605.
(13) Chemseddine, A.; Weller, H. *Ber. Bunsen-Ges. Phys. Chem.* **1993**, *97*, 636.
(14) Murray, C. B.; Norris, D. J.; Bawendi, M. G. *J. Am. Chem. Soc.* **1993**, *115*, 8706.
(15) Dance, I. G.; Choy, A.; Scudder, M. L. *J. Am. Chem. Soc.* **1984**, *106*, 6285.
(16) Herron, N.; Calabrese, J. C.; Farneth, W. E.; Wang, Y. *Science* **1993**, *259*, 1426.
(17) Turro, N. J. *Molecular Photochemistry*; W. A. Benjamin, Inc.: Reading, MA, 1965.
(18) Thomas, D. G.; Hopfield, J. J. *Phys. Rev.* **1959**, *116*, 573.
(19) Dameron, C. T.; Reese, R. N.; Mehra, R. K.; Kortan, A. R.; Carroll, P. J.; Steigerwald, M. L.; Brus, L. E.; Winge, D. R. *Nature* **1989**, *338*, 596.
(20) Katsikas, L.; Eychmüller, A.; Giersig, M.; Weller, H. *Chem. Phys. Lett.* **1990**, *172*, 201.
(21) Lee, G. S. H.; Craig, D. C.; Ma, I.; Scudder, M. L.; Bailey, T. D.; Dance, I. G. *J. Am. Chem. Soc.* **1988**, *110*, 4863.
(22) Strickler, P. *Chem. Commun.* **1969**, 655.
(23) Schwarzenbach, G.; Gautschi, K.; Peter, J.; Tunaboylu, K. *Trans. R. Inst. Technol. Stockholm* **1972**, *271*, 295.
(24) Lee, G. S. H.; Fisher, K. J.; Craig, D. C.; Scudder, M. L.; Dance, I. G. *J. Am. Chem. Soc.* **1990**, *112*, 6435.
(25) Rama Krishna, M. V.; Friesner, R. A. *J. Chem. Phys.* **1991**, *95*, 8309.
(26) Lippens, P. E.; Lannoo, M. *Phys. Rev. B* **1989**, *39*, 10935.
(27) Schooss, D.; Mews, A.; Eychmüller, A.; Weller, H. *Phys. Rev. B*, in press.
(28) Kayanuma, Y. *Phys. Rev. B* **1988**, *38*, 9797.
(29) Brus, L. E. *J. Chem. Phys.* **1984**, *80*, 4403.
(30) Rajh, T.; Micic, O. I.; Nozik, A. J. *J. Phys. Chem.* **1993**, *97*, 11999.
(31) Radkowsky, A. *Phys. Rev.* **1948**, *73*, 749.
(32) Fan, H. Y. *Phys. Rev.* **1951**, *82*, 900.
(33) Bleil, C. E.; Broser, I. *Proceedings of the Seventh International Conference on the Physics of Semiconductors, Paris 1964*, Dunod, Paris, 1964; p 897.
(34) Anedda, A.; Fortin, E. *Phys. Status Solidi A* **1976**, *36*, 385.
(35) Norris, D. J.; Nirmal, M.; Murray, C. B.; Sacra, A.; Bawendi, M. B. *Z. Phys. D* **1993**, *26*, 355.
(36) Shiang, J. J.; Risbud, S. H.; Alivisatos, A. P. *J. Chem. Phys.* **1993**, *98*, 8432.
(37) Schoenlein, R. W.; Mittleman, D. M.; Shiang, J. J.; Alivisatos, A. P.; Shank, C. V. *Phys. Rev. Lett.* **1993**, *70*, 1014.